Chemically Induced Multiplet Electron−Nuclear Polarization in Zero and Low Magnetic Fields

Elena G. Bagryanskaya,*,† Haruhiko Yashiro,‡ Matvei Fedin,† Peter Purtov,§ and Malcolm D. E. Forbes‡

International Tomography Center, Siberian Branch, Russian Academy of Sciences, Novosibirsk 630090, Russia, Institute of Chemical Kinetics and Combustion, Siberian Branch, Russian Academy of Sciences, Novosibirsk 630090, Russia, and Venable and Kenan Laboratories, Department of Chemistry, CB #3290, University of North Carolina, Chapel Hill, North Carolina 27599

We report the first observation of chemically induced electronic−nuclear multiplet spin polarization of transient radicals at very low and zero magnetic fields. Dimethoxyphosphonyl radicals, which have a hyperfine coupling constant of ∼70 mT, were produced in solution by photolysis of 2,4,6-trimethylbenzoyl phosphonic acid dimethyl ester. The radicals were detected using a modified L-band time-resolved electron paramagnetic resonance (TREPR) setup. The polarization is very strong, and signals are easily detected with custom-built resonators that match or nearly match each electronic−nuclear transition. A theoretical description for the formation of this large polarization has been proposed and is found to be in good agreement with experimental data. TREPR spectra and time-resolved kinetics at low and high magnetic fields have been measured. Signals detected at high magnetic field decay an order of magnitude faster than do those at low field, which can be explained by field-dependent HFI-induced spin relaxation.

I. Introduction

Chemically induced electron spin polarization (CIDEP) of reactive radicals is a well-known phenomenon and can arise from a variety of mechanisms such as the triplet mechanism (TM), radical pair mechanism (RPM), spin-correlated radical pair mechanism (SCRP), radical triplet pair mechanism (RTPM), or via cross-relaxation.[1−4] All of these mechanisms have been extensively investigated by time-resolved electron paramagnetic resonance (TREPR) spectroscopy at magnetic fields much higher than for the typical values of hyperfine interactions (HFI) of organic free radicals. At lower fields, L-band ($B_0 \approx 50$ mT) TREPR studies have been performed for carbon-centered radicals with small HFI constants (not exceeding 2.5 mT).[4−6] In these previous studies, an accurate experimental investigation of L-band CIDEP showed that there is a significant contribution of the S-T$_\pm$ CIDEP mechanism that manifests itself as a strong emissive component in the CIDEP spectra. Simulations of L-band CIDEP spectra and kinetics allow for quantitative study of magnetic field effects on TM and SCRP CIDEP.[5,6] A theoretical investigation of low-field CIDEP in radical pair recombination has been reported by Shushin.[7] He showed that the characteristic features of the low-field S-T$_\pm$ mechanism of CIDEP differ qualitatively from those predicted by the conventional high-field S-T$_-$ mechanism. This theoretical treatment was limited by the relatively strong magnetic fields B_0 used and the small hyperfine constant a ($a \ll \gamma_e B_0$).

During the past decade, several articles have been published regarding the influence of weak constant and radio-frequency

magnetic fields on chemical reactions, especially in the biologically relevant systems.[8] It has been shown that among the major factors determining the scales of the possible effects are the spin relaxation rates of the individual radicals as well as the initial nonequilibrium populations of the spin levels. At low magnetic fields, particularly those fields that are comparable to the hyperfine coupling constants of the radicals, the spin eigenfunctions of the radicals can no longer be represented as products of electronic and nuclear wave functions. The resonant transitions for such a system are not purely electronic or nuclear, which leads to some special spectral features that are due to the effect of rf fields on the nuclear polarization of the diamagnetic reaction products. Recently, it has been shown[9] that low-field electronic−nuclear transitions can be detected via nuclear polarization of the diamagnetic products. These experiments revealed very high nonequilibrium populations of the spin levels in magnetic fields comparable to and lower than the value of the HFI constants of the intermediate radicals ($\gamma_e B_0 < a$). In this article, we report the first experiments involving direct measurement of low magnetic field chemically induced spin polarization using TREPR. Very large multiplet electronic−nuclear spin polarization, which we call ENP, has been observed in low and even zero magnetic fields and is remarkably strong. To explain these results, a theory has been developed that proposes a mechanism for the formation and decay of spin polarization in low and zero magnetic fields.

II. Theory

1. Basic Features of Low-Field TREPR. The eigenfunctions and eigenstates for a radical containing one magnetic nucleus ($I = {}^1/_2$) with HFI constant a are expressed by the Breit−Rabi formulas:[10]

* To whom correspondence should be addressed. E-mail: elena@tomo.nsc.ru.
† International Tomography Center, Russian Academy of Sciences.
‡ University of North Carolina.
§ Institute of Chemical Kinetics and Combustion, Russian Academy of Sciences.

Multiplet Electron−Nuclear Polarization

J. Phys. Chem. A, Vol. 106, No. 12, 2002 **2821**

$$|1\rangle = |\alpha_e\alpha_n\rangle, \qquad E_1 = \frac{\omega_e}{2} + \frac{a}{4}$$

$$|2\rangle = C_1|\alpha_e\beta_n\rangle + C_2|\beta_e\alpha_n\rangle, \qquad E_2 = -\frac{a}{4} + \frac{\sqrt{\omega_e^2 + a^2}}{2}$$

$$|3\rangle = |\beta_e\beta_n\rangle, \qquad E_3 = -\frac{\omega_e}{2} + \frac{a}{4}$$

$$|4\rangle = C_2|\alpha_e\beta_n\rangle - C_1|\beta_e\alpha_n\rangle, \qquad E_4 = -\frac{a}{4} - \frac{\sqrt{\omega_e^2 + a^2}}{2} \tag{1}$$

where $C_1^2 = {}^1\!/_2(1 + (\omega_e/\sqrt{\omega_e^2 + a^2}))$ and $C_2^2 = {}^1\!/_2(1 - (\omega_e/\sqrt{\omega_e^2 + a^2}))$. Here, $\omega_e = \gamma_e B_0$ is the Zeeman frequency of the electron and γ_e is the electron gyromagnetic ratio. In low magnetic fields (B_0), all the transitions occur with the participation of both nuclear and electronic spins. The probability of a transition under the influence of a resonant magnetic field B_1 is proportional to

$$P_{1\leftrightarrow2} \sim |\langle1|\hat{B}_{1x}(\gamma_e\hat{S}_x + \gamma_n\hat{I}_x)|2\rangle|^2 =$$
$$B_1^2(C_1^2\gamma_n^2 + C_2^2\gamma_e^2) \approx B_1^2 C_2^2\gamma_e^2$$

$$P_{1\leftrightarrow4} \sim |\langle1|\hat{B}_{1x}(\gamma_e\hat{S}_x + \gamma_n\hat{I}_x)|4\rangle|^2 =$$
$$B_1^2(C_2^2\gamma_n^2 + C_1^2\gamma_e^2) \approx B_1^2 C_1^2\gamma_e^2$$

$$P_{1\leftrightarrow2} = P_{3\leftrightarrow4}$$

$$P_{1\leftrightarrow4} = P_{2\leftrightarrow3} \tag{2}$$

The squared coefficients C_1^2 and C_2^2 are 1 and 0 in high magnetic fields, respectively, where these transitions are purely nuclear or electronic. At zero magnetic field, the squared coefficients are 0.5 because the transitions occur with the simultaneous flip of electronic and nuclear spins. An additional phenomenon in low magnetic fields is the induction of another transition, $|2\rangle\leftrightarrow|4\rangle$, when the rf field is parallel to the external magnetic field. The probability of this transition is proportional to

$$P_{2\leftrightarrow4} \sim |\langle2|\hat{B}_{1z}(\gamma_e\hat{S}_z + \gamma_n\hat{I}_z)|4\rangle|^2 =$$
$$B_1^2(C_1^2 C_2^2\gamma_n^2 + C_1^2 C_2^2\gamma_e^2) \approx B_1^2 C_1^2 C_2^2\gamma_e^2 \tag{3}$$

2. Formation of Spin Polarization in Low and Zero Magnetic Fields.

The initial spin-level populations of the radicals that escaped to the bulk strongly depend on the conditions under which the radicals have separated, which affects the magnitude of the geminate ENP. The separation can be adiabatic or nonadiabatic depending on the radical size, solution viscosity, and the HFI constants. The criterion of adiabaticity can be written as $\lambda^2/D \sim a^{-1}$,[11] where a is the HFI constant, D is the mutual diffusion coefficient, and λ is the characteristic scale for exponential decay of the exchange interaction in its usual form: $J(r) = J_0 \exp(-(r - R)/\lambda)$ (R is the distance of closest radical approach). We now consider low-field ENP formation for two limiting cases of adiabatic ($\lambda^2/D \gg a^{-1}$) and nonadiabatic ($\lambda^2/D \ll a^{-1}$) RP separation.

Adiabatic Contribution. In the case of adiabatic separation, the population of each eigenstate remains the same at any moment in time, though the eigenfunctions themselves change
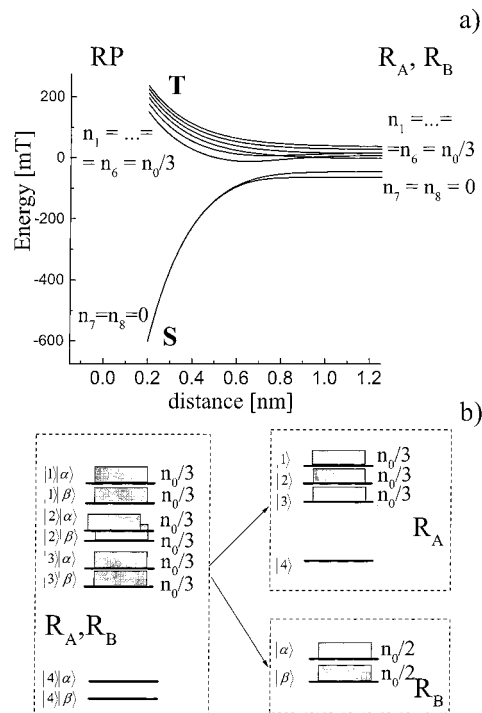

Figure 1. (a) Calculated scheme of the energy levels of RP with one magnetic nucleus as a function of interradical distance; $J(r) = J_0 \exp(-(r - R)/\lambda)$, $J_0 = 400$ mT, $R = 0.2$ nm, $\lambda = 0.2$ nm, $a = 70$ mT, and $B_0 = 20$ mT. (b) Correlation scheme for the RP- and radical-level populations.

significantly. Therefore, we can predict the initial populations of RP spin levels in a low magnetic field using the simple energy-level scheme shown in Figure 1a. We assume that the RP has been formed from a triplet precursor and that ENP due to the triplet mechanism is negligible. Under the condition that $J \gg a, \gamma_e B_0$, the six upper spin levels have equal populations, but the two lower levels are not populated. For the case when $a \gg \gamma_e B_0$, after adiabatic RP separation to the region where $J = 0$, the six upper spin levels also have equal populations, and the two lower levels are empty. At $J = 0$, the eigenfunctions can be presented as products of the eigenfunctions of the individual radicals. Therefore, one can easily calculate the populations of spin levels of each radical by summing over all spin states of the other one, as shown in Figure 1b. Hence, in the case of adiabatic RP separation, one should expect a large nonequilibrium population of the spin levels of radicals with magnetic nuclei. This electronic−nuclear polarization can be detected by applying a transverse or parallel resonant rf field at frequencies corresponding to transitions $|1\rangle\leftrightarrow|4\rangle,|3\rangle\leftrightarrow|4\rangle$ (transverse), and $|2\rangle\leftrightarrow|4\rangle$ (parallel).

For radicals with HFI constants of 1−2 mT in nonviscous solutions, the adiabatic contribution is negligible, but it can be important for RPs with large HFI constants in solutions of high viscosity (e.g. in micelles and for radical ion pairs).

Nonadiabatic Contribution. For this case, we introduce a density matrix $\hat{\rho}(\overline{q},t)$ in a basis containing all the electronic−nuclear spin states of the RP.[12,13] In ref 14, the CIDEP effect was calculated for the case of high magnetic field to a first approximation with respect to the exchange interaction. Here we use the same approach to calculate the ENP magnitude for the case of zero magnetic field. Although this approach involves rather cumbersome matrix algebra, it is more convenient than an exact numerical solution of the stochastic Liouville equation as it allows an analytical result.

2822 *J. Phys. Chem. A, Vol. 106, No. 12, 2002*

Bagryanskaya et al.

Multiplet ENP is determined by the product of operators of electronic and nuclear spins:

$$\langle \hat{S}_{Az}\hat{I}_z \rangle = Tr_{A,B}(\hat{S}_{Az}\hat{I}_z\hat{\rho}(t)) \qquad (4)$$

We consider an RP with one magnetic nucleus of spin $I = ^1/_2$. In both zero and low magnetic fields, the projection of the total spin onto the z-axis is conserved (i.e., $\hat{S}_{1z} + \hat{S}_{2z} + \hat{I}_z = $ constant). Consequently, the ensemble of RPs can be divided into four subensembles with the basis functions

  (I) $|T_+\alpha\rangle$
  (II) $|T_-\beta\rangle$
  (III) $|S\alpha\rangle$, $|T_0\alpha\rangle$, $|T_+\beta\rangle$
  (IV) $|S\beta\rangle$, $|T_0\beta\rangle$, $|T_-\alpha\rangle$

The first two subensembles do not take part in the spin evolution of the RP. The spin evolution of two last subensembles is similar at zero magnetic field; therefore, we present the theory only for subensemble (III).

As shown in ref 14, the CIDEP effect is expressed in terms of matrixes $\hat{\hat{T}}(t)$, $\hat{\hat{G}}_0(\vec{q},\vec{q}';s)$, and $\hat{\hat{G}}(\vec{q},\vec{q}';s)$ defined in that article where the matrix elements of $\hat{\hat{G}}_0(\vec{q},\vec{q}';s)$ are easily expressed in terms of $\hat{\hat{T}}(t)$. Spin evolution influenced by the isotropic HFI can be written as

$$\psi(t) = \hat{S}(t)\,\psi(0) = \exp(-i\hat{H}t/\hbar)\,\psi(0), \qquad \hat{H} = a\hat{S}\hat{I} \quad (5)$$

The matrix $\hat{S}(t)$ in basis (III) has the form

$$\hat{S}(t) = \begin{bmatrix} (e^{iat}+3)/4 & (e^{iat}-1)/4 & (-e^{iat}+1)/2\sqrt{2} \\ (e^{iat}-1)/4 & (e^{iat}+3)/4 & (-e^{iat}+1)/2\sqrt{2} \\ (-e^{iat}+1)/2\sqrt{2} & (-e^{iat}+1)/2\sqrt{2} & (e^{iat}+1)/2 \end{bmatrix} \quad (6)$$

In the Liouville representation, the basis states of subensemble (III) are $|S\alpha,S\alpha\rangle$, $|S\alpha,T_0\alpha\rangle$, $|T_0\alpha,S\alpha\rangle$, $|T_0\alpha,T_0\alpha\rangle$, $|S\alpha,T_+\beta\rangle$, $|T_+\beta,S\alpha\rangle$, $|T_0\alpha,T_+\beta\rangle$, $|T_+\beta,T_0\alpha\rangle$, and $|T_+\beta,T_+\beta\rangle$. The matrix elements of the Liouville evolution operator $\hat{\hat{T}}(t)$ are expressed through the matrix elements of operator $\hat{S}(t)$ as

$$\hat{\hat{T}}_{ij,lm}(t) = \hat{S}_{il}(t)\cdot\hat{S}^*_{jm}(t) \qquad (7)$$

To calculate $\bar{G}(\vec{q},\vec{q}';s)$, we need an expression for the operator for the exchange interaction, which in the Liouville basis has four nonzero matrix elements:

$$-\langle S\alpha,T_0\alpha|\hat{\hat{J}}(\vec{q})|S\alpha,T_0\alpha\rangle = \langle T_0\alpha,S\alpha|\hat{\hat{J}}(\vec{q})|T_0\alpha,S\alpha\rangle = $$
$$-\langle S\alpha,T_+\beta|\hat{\hat{J}}(\vec{q})|S\alpha,T_+\beta\rangle = \langle T_+\beta,S\alpha|\hat{\hat{J}}(\vec{q})|T_+\beta,S\alpha\rangle = 2J(r) \quad (8)$$

Therefore, the diagonal matrix $\hat{\hat{G}}(\vec{q},\vec{q}';s)$ has the following features:

$$\langle S\alpha,T_0\alpha|\hat{\hat{G}}(\vec{q})|S\alpha,T_0\alpha\rangle = \langle T_0\alpha,S\alpha|\hat{\hat{G}}^*(\vec{q})|T_0\alpha,S\alpha\rangle = $$
$$\langle S\alpha,T_+\beta|\hat{\hat{G}}(\vec{q})|S\alpha,T_+\beta\rangle = \langle T_+\beta,S\alpha|\hat{\hat{G}}^*(\vec{q})|T_+\beta,S\alpha\rangle \equiv$$
$$\bar{G}(\vec{q},\vec{q}';s) \quad (9)$$

All the other diagonal elements are equal functions $G(\vec{q},\vec{q}';s)$. We use here the same designations for $\bar{G}(\vec{q},\vec{q}';s)$ and $G(\vec{q},\vec{q}';s)$ as are used in ref 14.

To understand the origin of the ENP effect, we consider an RP formed in a triplet state without taking into account chemical

recombination. For a radical with one magnetic nucleus, the mean values of the spin state populations can be written as

$$n_1 = \frac{1}{4} - Re\rho_{S\alpha,T_0\alpha}$$

$$n_2 = \frac{1}{4} + \frac{1}{\sqrt{2}}(Re\rho_{S\alpha,T_+\beta} - Re\rho_{S\beta,T_-\alpha}) +$$
$$\frac{1}{2}(Re\rho_{S\alpha,T_0\alpha} - Re\rho_{S\beta,T_0\beta})$$

$$n_3 = \frac{1}{4} + Re\rho_{S\beta,T_0\beta}$$

$$n_4 = \frac{1}{4} - \frac{1}{\sqrt{2}}(Re\rho_{S\alpha,T_+\beta} - Re\rho_{S\beta,T_-\alpha}) +$$
$$\frac{1}{2}(Re\rho_{S\alpha,T_0\alpha} - Re\rho_{S\beta,T_0\beta}) \quad (10)$$

where $\rho_{S\alpha,T_0\alpha}$, $\rho_{S\alpha,T_+\beta}$, $\rho_{S\beta,T_-\alpha}$, and $\rho_{S\beta,T_0\beta}$ are the mean values of the nondiagonal elements of the density matrix of the RP in the absence of recombination. These terms appear because of exchange and hyperfine interactions.

Direct calculations show that at zero magnetic field the following relations hold:

$$Re\rho_{S\beta,T_0\beta} = -Re\rho_{S\alpha,T_0\alpha}; \qquad Re\rho_{S\beta,T_-\alpha} = -Re\rho_{S\alpha,T_+\beta} \quad (11)$$

Substituting eq 11 into eq 10, we obtain

$$n_1 = \frac{1}{4} - Re\rho_{S\alpha,T_0\alpha}$$

$$n_2 = \frac{1}{4} + Re\rho_{S\alpha,T_0\alpha} + \sqrt{2}Re\rho_{S\alpha,T_+\beta}$$

$$n_3 = \frac{1}{4} - Re\rho_{S\alpha,T_0\alpha}$$

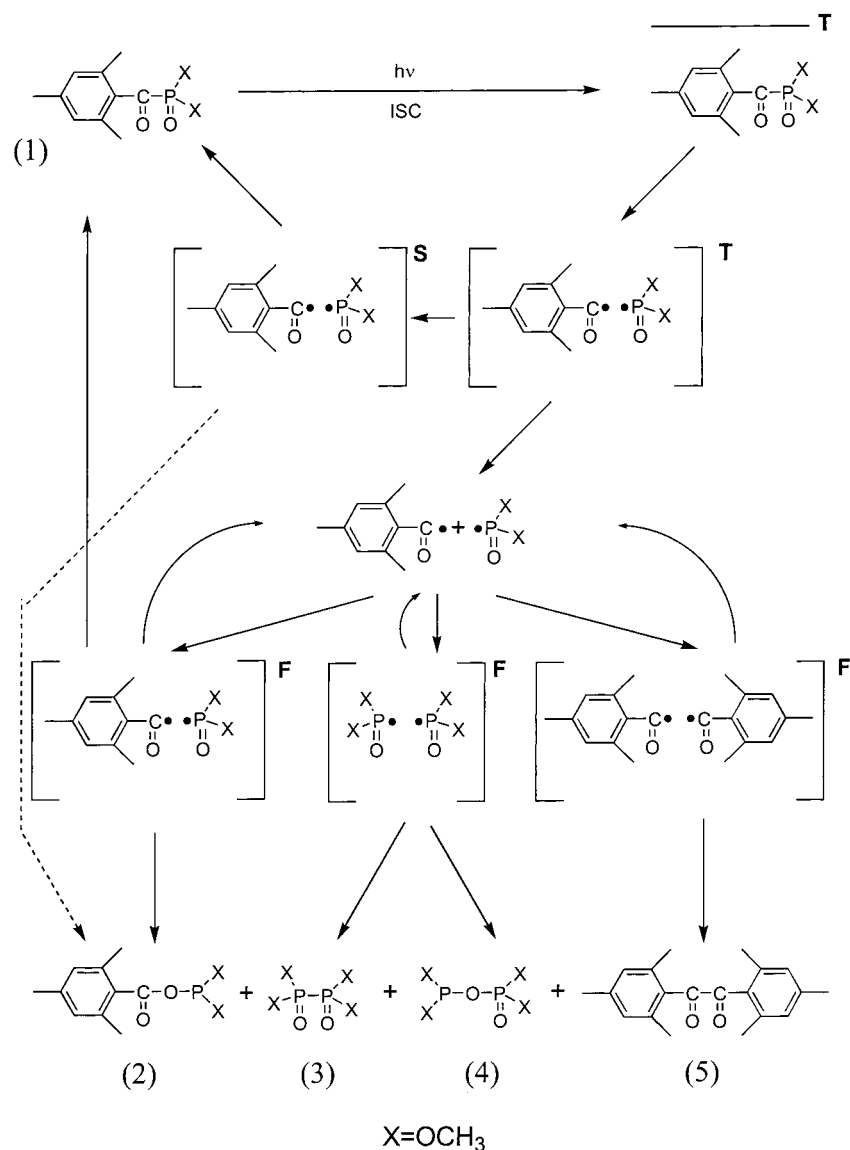$$n_4 = \frac{1}{4} + Re\rho_{S\alpha,T_0\alpha} - \sqrt{2}Re\rho_{S\alpha,T_+\beta} \quad (12)$$

Thus, the calculation of the populations requires the knowledge of only two nondiagonal elements, using the approach detailed in ref 14, and the matrixes $\hat{\hat{T}}(t)$ and $\hat{\hat{G}}(\vec{q},\vec{q}';s)$ described above. For nonviscous solutions, we obtain the following result:

$$Re\rho_{S\alpha,T_0\alpha} = -\frac{\sqrt{a\tau_d}}{48\sqrt{2}} - \frac{\sqrt{a\tau_j}}{48\sqrt{2}}(\pi + \ln|J_0\tau_j| + 2\gamma)$$

$$Re\rho_{S\alpha,T_+\beta} = \frac{\sqrt{a\tau_d}}{48} + \frac{\sqrt{a\tau_j}}{48}(\pi + \ln|J_0\tau_j| + 2\gamma) \quad (13)$$

where $\tau_j = \lambda^2/D$, $\tau_d = R^2/D$, and $\gamma \cong 0.577$ is the Euler constant. The expressions in eq 13 have been obtained for the case $a\tau_d$, $a\tau_j \ll 1$, corresponding to nonviscous solutions and assuming that $a > 0$ and $J < 0$. Substituting eq 13 into eq 12, we obtain the final expression for the populations:

$$n_1 = n_2 = n_3 = \frac{1}{4} + \frac{\sqrt{a\tau_d}}{48\sqrt{2}} + \frac{\sqrt{a\tau_j}}{48\sqrt{2}}(\pi + \ln|J_0\tau_j| + 2\gamma)$$

$$n_4 = \frac{1}{4} - \frac{\sqrt{a\tau_d}}{16\sqrt{2}} - \frac{\sqrt{a\tau_j}}{16\sqrt{2}}(\pi + \ln|J_0\tau_j| + 2\gamma) \quad (14)$$

Multiplet Electron−Nuclear Polarization

J. Phys. Chem. A, Vol. 106, No. 12, 2002 **2823**

SCHEME 1: Photolysis of TMPDE in a Homogeneous Solution

$X = OCH_3$

For an HFI constant of 70 mT (corresponding to the dimethoxyphosphonyl radical used in our experiments) and assuming that $\lambda = 0.05$ nm, $R = 0.4$ nm, and $D = 5 \times 10^{-5}$ cm^2/s, we calculate $\tau_j = 0.5$ ps and $\tau_d = 32$ ps. Taking the reasonable value $\ln|J_0\tau_j| \approx 1$, we obtain $n_1 = n_2 = n_3 = 0.265$ and $n_4 = 0.204$. Thus, at zero magnetic field, $n_1 - n_4 = n_2 - n_4 = n_3 - n_4 = 0.061$, whereas $a/kT \approx 10^{-4}$, which means that a large emissive line should be observed, corresponding to transitions $|1\rangle$, $|2\rangle$, $|3\rangle \leftrightarrow |4\rangle$ with nonequilibrium populations of the spin levels.

Thus, one can see that the adiabatic and nonadiabatic contributions each lead to a similar pattern for the initial populations of a radical containing a magnetic nucleus at low and zero magnetic fields. Both mechanisms predict the three upper spin levels $|1\rangle$, $|2\rangle$, and $|3\rangle$ to be more populated than the lower spin level $|4\rangle$.

III. Experimental Section

In this study, we have created RPs using the photolysis of 2,4,6-trimethylbenzoyl phosphonic acid dimethyl ester (TMPDE, in Scheme 1), which undergoes α scission upon irradiation with UV light, with a quantum yield of $\phi(\alpha) = 0.3$.[15] Photolysis occurs from the excited triplet state and forms triplet radical

pairs of phosphonyl and acyl radicals. Chemical decay of the intermediate radicals is determined by the recombination rate of radicals in the bulk. The second-order rate constant for self-termination of two dimethoxyphosphonyl radicals is close to the diffusion-controlled limit[15] (i.e., about 3.3×10^9 M^{-1} s^{-1} in di-*tert*-butyl peroxide at 253 K[15]). The rate constant for cross-termination of the phosphorus-centered species with trimethylbenzoyl radicals should be very close to that of the self-termination reaction. The radical $(CH_3O)_2(O)P^{\bullet}$ has a large HFI of $a[^{31}P] \approx 70$ mT and small HFI constants of $a[^1H] = 0.05$ mT for the six methyl protons.[16] It is the large value of the HFI constant of the ^{31}P nucleus that allows us to use L-band TREPR with resonance close to 2 GHz to investigate the transitions at very low and zero magnetic fields.

A JEOL L-band TREPR setup has been modified for these measurements. To increase the sensitivity, a GaAs MW ampli-fier (Miteq AMF-4F-011018-04-13P) has been inserted before a double-balanced mixer detector. The TREPR signal was amplified by a wideband preamplifier (0.5 Hz−50 MHz). Homemade loop gap resonators with an approximate Q factor of 200 were used to obtain a balance between high sensitivity and fast time resolution. To measure the signals at zero magnetic field, the resonant frequencies of the cavities were fine-tuned
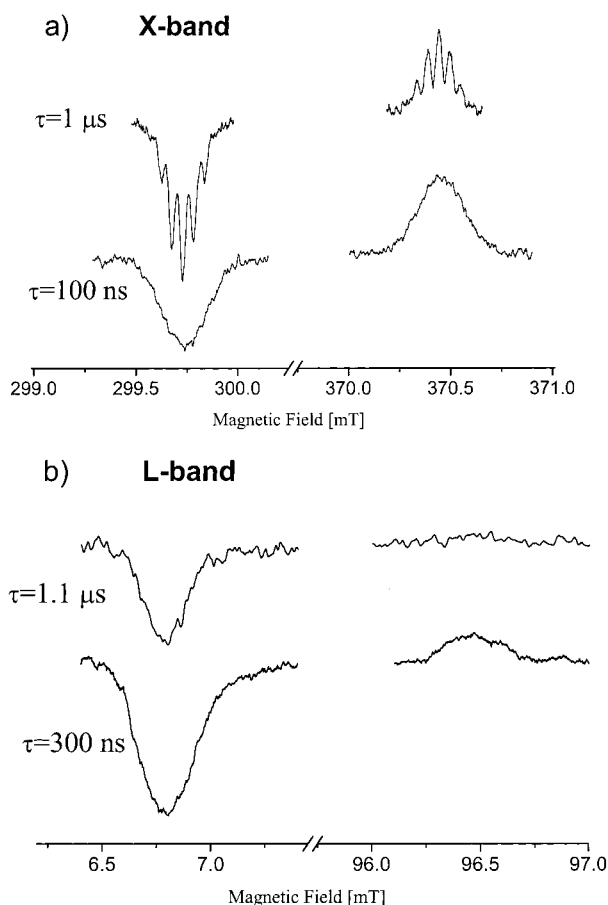
a) **X-band**

Figure 2. CIDEP spectra of the dimethoxyphosphonyl radical (MeO)$_2$(O)P$^\bullet$ in acetonitrile at room temperature in the (a) X band and the (b) L band.

over ranges of about 10 MHz by changing the distance between the copper plate and the capacitive split in the resonator.

IV. Results and Discussion

X- and L-Band Spectra. Figures 2a and b show CIDEP spectra at X and L bands, respectively, obtained at different time delays after laser photolysis of TMPDE in acetonitrile solution at room temperature. The spectra show an E/A pattern assigned to the dimethoxyphosphonyl radical. The polarization of the acyl radical is not observed. The line positions are in good agreement with those from the calculated low-field (f = 1.9804 GHz) EPR spectrum for a radical with one HFI constant, a = 70.44 mT. The high-field EPR line in the L-band spectra could not be detected at long time delays because of an insufficient signal/noise ratio. At the X band, the hyperfine structure of the six hydrogen atoms is well-resolved, but at the L band, the line width is approximately 0.3 mT and these six hydrogen atoms' couplings are unresolved. For high field, the resonance frequency is proportional to the magnetic field $\omega_0 = \gamma_e B_0$, but for low magnetic fields, the relationship becomes more complex. For example, the energy gap for the $|1\rangle \leftrightarrow |4\rangle$ transition is $\Delta E = (\gamma_e B_0 + a + \sqrt{(\gamma_e B_0)^2 + a^2})/2$. One can see that $(d\Delta E/dB_0)$ (when $B_0 \gg a$) = $\gamma_e = 2(d\Delta E/dB_0)$ (when $B_0 \ll a$). Hence, for a fixed frequency ω, a Lorentzian line $g(B_0) = 1/(1 + (\Delta E - \omega)^2 T_2^2)$ is expected to be 2 times broader at low magnetic fields than at high fields for equal values of T_2. The same is true for the $|2\rangle \leftrightarrow |3\rangle$ transition. On the other hand, as has been shown in ref 17, the EPR line width due to anisotropic HFI-induced relaxation decreases in low magnetic fields (i.e.,
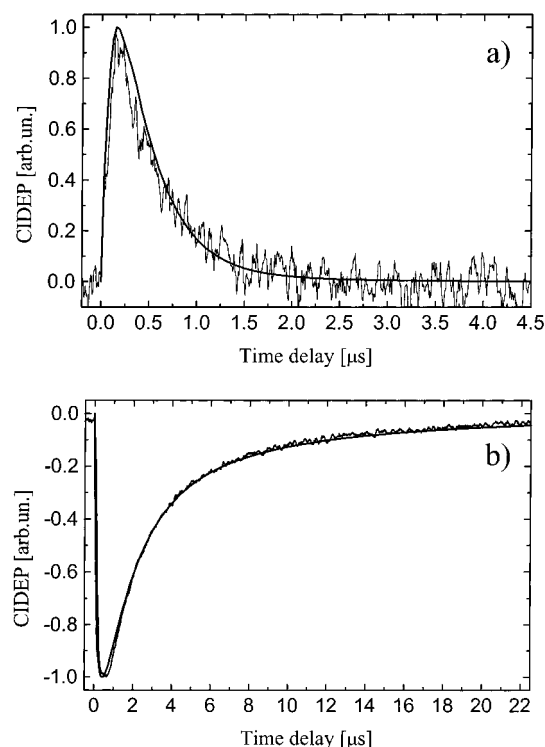

Figure 3. Experimental kinetics and simulation of CIDEP kinetics detected by high-field (a) and low-field (b) EPR lines in the transversal magnetic field $B_1 \perp B_0$. The kinetics have been calculated for the following set of parameters: [A:A] = 176 mT^2, τ_c = 2.4 ps, $2k_tR_0 = 3.2 \times 10^5$ s^{-1}, $B_1 = 10^{-4}$ mT, B_0 = 96.2 mT (a), B_0 = 4.4 mT (b).

T_2 is different in high and low magnetic fields). But the decrease of the line width due to the difference in phase relaxation does not exceed ∼30%;[17] therefore, the broadening predominates. Thus, the difference in the line width of the dimethoxyphosphonyl radical between the X and L bands can be explained by the broadening of each line of HFI structure at low field.

TREPR Kinetics for $B_1 \perp B_0$. Figures 3a and b show TREPR kinetics measured for both emissive and absorptive lines. It has been found that the kinetics of the low-field emissive line decay much slower than those of the high-field line at the same laser intensity. The decay at high field is approximately monoexponential, whereas the decay at low field is better described by second-order kinetics. This result can be explained by the nature of HFI-induced spin relaxation at low fields and is in complete agreement with our recent theoretical article.[17] It was shown there that at low field the relaxation rate between the lower and the three upper spin levels ($|1\rangle$, $|2\rangle$, $|3\rangle \leftrightarrow |4\rangle$) is expected to be very slow in comparison with that at high field. The HFI-induced relaxation rate between levels $|1\rangle$, $|2\rangle$, $|3\rangle \leftrightarrow |4\rangle$ decreases to zero at zero magnetic field because relaxation transitions induced by dipole−dipole interactions are not allowed between states that have different total spins.

On the basis of the results from ref 17, using a = 70 mT, a fluctuation amplitude due to hyperfine anisotropy, [A:A] = 176 mT^2, and τ_c=2.4 ps, we estimate that the HFI-induced relaxation time will be ∼500 μs at B_0 = 4.4 mT. Therefore, we conclude that the high-field TREPR kinetics shown in Figure 3a are determined by HFI-induced spin relaxation, whereas the low-field kinetics (Figure 3b) are determined by a chemical reaction.

These conclusions have been confirmed by the calculated kinetic traces shown in Figure 3, which were generated using a numerical solution of the Stochastic Liouville equation via a Laplace transform. Details are given in the Appendix. The
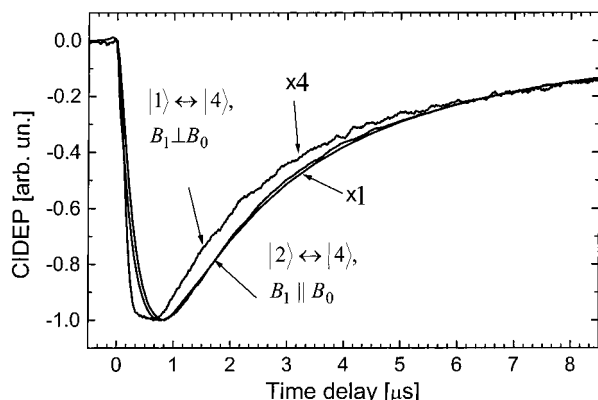
Multiplet Electron−Nuclear Polarization

J. Phys. Chem. A, Vol. 106, No. 12, 2002 **2825**

Figure 4. Experimental kinetics and simulation of CIDEP kinetics detected by the $|2\rangle\leftrightarrow|4\rangle$ EPR lines in the parallel magnetic field $B_1\|B_0$ and comparison with the $|1\rangle\leftrightarrow|4\rangle$ low-field line obtained using $B_1\perp B_0$. The kinetics have been calculated for the following set of parameters: [A:A] = 176 mT², τ_c = 2.4 ps, B_0 = 5.0 mT, B_1 = 10^{-4} mT, $2k_tR_0$ = 3×10^5 s⁻¹.

correlation time for radical rotation and the initial radical concentration were the variable parameters. Both kinetic traces shown in Figure 3 were calculated using the same set of parameters listed in the caption. The correlation time of 2.4 ps agrees well with that determined for the (EtO)₂(O)P• radical in di-*tert*-butyl peroxide (∼5 ps).[18,19]

TREPR Kinetics for $B_1\|B_0$. Figure 4 shows the TREPR kinetics of the $|2\rangle\leftrightarrow|4\rangle$ transition induced by a microwave field parallel to the external magnetic field of 0.5 mT. The observed kinetic trace shows the same features as the kinetics of the $|1\rangle\leftrightarrow|4\rangle$ low-field transition discussed above. The decay is determined by a second-order chemical reaction. It is interesting that the extremum of the kinetic trace obtained using $B_1\|B_0$ is shifted for ∼300 ns to longer time delays in comparison with that of the kinetics obtained using $B_1\perp B_0$ (Figure 3). At the same time, a best fit to the experimental kinetics for $B_1\|B_0$ was obtained using the same set of parameters as that used in the

simulations of kinetics for $B_1\perp B_0$. The position of the extremum of the kinetic trace for the small values of B_1 used here is determined by the relaxation rate, the chemical decay rate, and the initial populations of the spin levels. In our calculations, the initial populations of the three upper spin levels are assumed to be equal in both cases. Therefore, we propose that the shift of the extremum for $B_1\|B_0$ is caused by the different relaxation times for the $|1\rangle\leftrightarrow|4\rangle$ and the $|2\rangle\leftrightarrow|4\rangle$ transitions, in agreement with ref 17.

Spin Polarization at Zero Magnetic Field. Figure 5a shows the emissive signal of the dimethoxyphosphonyl radical observed using rf frequencies close to the value of the HFI constant f_{hfi}(70.44 mT) = 1.972 GHz. The magnetic field was swept gradually from −1.0 to 1.0 mT to detect the resonant transition at zero magnetic field. The observed lines correspond to the transition $|1\rangle\leftrightarrow|4\rangle$ when $f > f_{hfi}$ and to the transition $|3\rangle\leftrightarrow|4\rangle$ when $f < f_{hfi}$. At very low magnetic fields, $B_0 < 1.0$ mT, the intensities of both lines are approximately equal. One can see that the $|3\rangle\leftrightarrow|4\rangle$ transition is a bit broader than the $|1\rangle\leftrightarrow|4\rangle$ transition when $f \approx f_{hfi}$. This feature is well-reproduced by the calculations shown in Figure 5b. As has been discussed above, the line width at low field is determined by the unresolved HFI structure of six hydrogens, and the calculated positions of these unresolved maxima are slightly different for the $|3\rangle\leftrightarrow|4\rangle$ and the $|1\rangle\leftrightarrow|4\rangle$ lines. It is very important to note that even at zero magnetic field a strongly emissive ENP line can be observed. In fact, its intensity is twice as large as that of each of the $|3\rangle\leftrightarrow|4\rangle$ and $|1\rangle\leftrightarrow|4\rangle$ lines, which reveals an opportunity to use the CIDEP technique to study free radical reactions at zero and very low magnetic fields.

Transition Intensities. The difference in line intensities between low field ($B_1\perp B_0$) and zero field has a clear explanation. If B_0 is equal to zero, the difference between the transverse and parallel directions of the rf field disappears, and the three transitions $|4\rangle\leftrightarrow|1\rangle$, $|2\rangle$, $|3\rangle$ all contribute to the overall intensity.
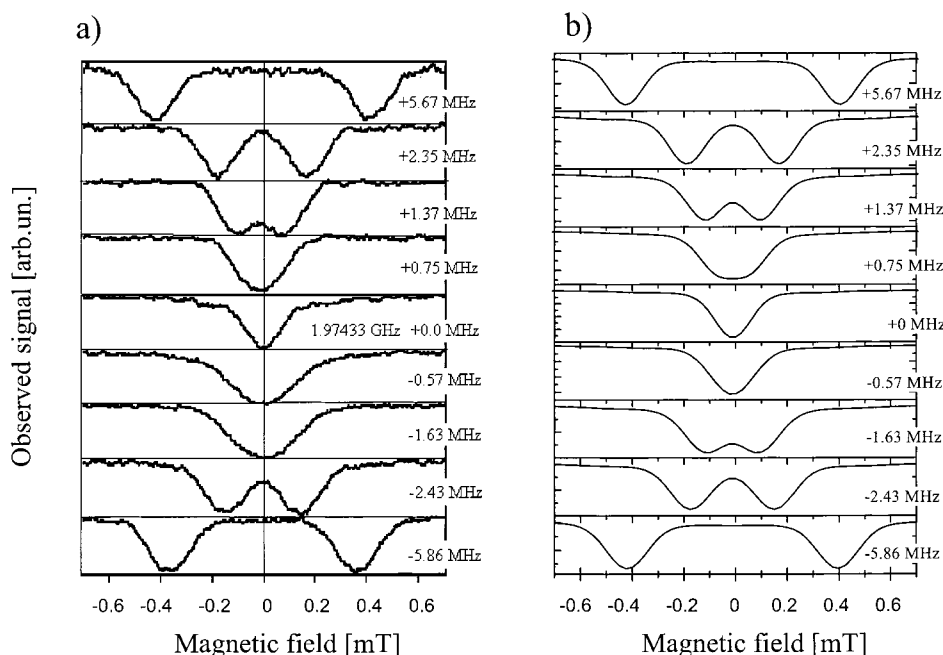

Figure 5. Experimental (a) and calculated (b) EPR spectra in low and zero magnetic fields at different frequencies of the applied rf field. The calculations have been made for $a[^{31}P]$ = 70.0 mT and six HFI constants $a[^1H]$ = 0.05 mT that determine the nonhomogeneously broadened line width.

2826 *J. Phys. Chem. A, Vol. 106, No. 12, 2002*

Bagryanskaya et al.

The probability of the transverse rf field-induced transition can be calculated as

$$P_\perp = P_{1\leftrightarrow4} = |\langle 1|\gamma_e B_{1x}S_x|4\rangle|^2 =$$
$$\left|\left\langle \alpha_e\alpha_n\left|\frac{\gamma_e B_{1x}(S_+ + S_-)}{2}\right|\frac{1}{\sqrt{2}}(\beta_e\alpha_n - \alpha_e\beta_n)\right\rangle\right|^2 =$$
$$\frac{\gamma_e^2 B_{1x}^2}{8} = P_{3\leftrightarrow4} \quad (15)$$

and the parallel rf field-induced transition is

$$P_\parallel = P_{2\leftrightarrow4} = |\langle 2|\gamma_e B_{1z}S_z|4\rangle|^2 =$$
$$\left|\left\langle \frac{1}{\sqrt{2}}(\alpha_e\beta_n + \beta_e\alpha_n)\left|\gamma_e B_{1z}S_z\right|\frac{1}{\sqrt{2}}(\beta_e\alpha_n - \alpha_e\beta_n)\right\rangle\right|^2 =$$
$$\frac{\gamma_e^2 B_{1z}^2}{4} \quad (16)$$

At zero magnetic field, there is not a single axis of quantization, and only the mutual orientation of the electronic and nuclear spins in each individual radical is important. Hence, when averaging over the whole ensemble of the radicals, for one-third of them, the applied microwave field can be considered to be x-directed, for one-third, y-directed, and for one-third, z-directed. For the cases where B_1 is x- and y-directed, two transitions ($|3\rangle\leftrightarrow|4\rangle$ and $|1\rangle\leftrightarrow|4\rangle$) are induced. For the case of z-directed B_1, only one transition ($|2\rangle\leftrightarrow|4\rangle$) is induced. Thus, the probability of a zero-field transition can be calculated as a sum:

$$P_0 = (2P_\perp)_x + (2P_\perp)_y + (P_\parallel)_z =$$
$$\gamma_e^2(B_{1x}^2 + B_{1y}^2 + B_{1z}^2)/4 = \gamma_e^2 B_1^2/4 = 2P_\perp \quad (17)$$

(i.e., the intensity of the zero-field line is two times larger than that of each of the transitions induced by the transverse rf field).

An interesting observation is that the measured ratio of amplitudes of transverse and parallel lines at the same external magnetic field is not in agreement with that from eqs 15 and 16. This ratio was measured using the signal in zero magnetic field for calibration. In fact, the amplitude of the $|2\rangle\leftrightarrow|4\rangle$ line is approximately 4 times larger than that of each of the $|1\rangle,|3\rangle\leftrightarrow|4\rangle$ lines. A possible explanation is that the population of level $|2\rangle$ is larger than the populations of levels $|1\rangle$ and $|3\rangle$, but this result can hardly be expected, as we showed in the theoretical section. The most reasonable explanation is the contribution of the hyperfine structure from the six additional hydrogens. Figure 6 shows an energy-level scheme for a radical containing one HFI constant of 70.0 mT and six HFI constants of 0.05 mT. One can see that the levels $|1\rangle$ and $|3\rangle$ are much broader than $|2\rangle$ and $|4\rangle$, thus the nonhomogeneously broadened $|1\rangle$, $|3\rangle\leftrightarrow|4\rangle$ lines should be much wider than the $|2\rangle\leftrightarrow|4\rangle$ line. In experiments using a parallel microwave field, it was not possible to measure the line width of the $|2\rangle\leftrightarrow|4\rangle$ transition by scanning the magnetic field or the frequency. The former is impossible, in principle, because the energy gap between spin levels $|2\rangle$ and $|4\rangle$ is almost constant with magnetic field for $B_0 \ll a$. Measurement of the latter led to technical difficulties, but discrete measurements at different $f \approx f_{2\leftrightarrow4}$ showed that the $|2\rangle\leftrightarrow|4\rangle$ line is very narrow, in agreement with Figure 6. Consequently, the amplitude of the narrow $|2\rangle\leftrightarrow|4\rangle$ line should be more than 2 times greater than that of the $|1\rangle$, $|3\rangle\leftrightarrow|4\rangle$ lines because of unresolved HFI structure.
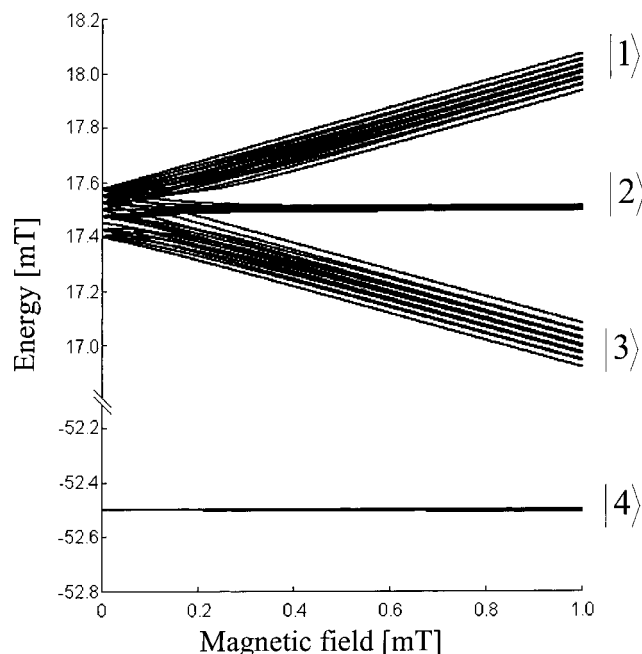

Figure 6. Calculated scheme of the energy spin levels for the radical with one HFI constant $a[^{31}P] = 70.0$ mT and six HFI constants $a[^1H] = 0.05$ mT.

Comparison with TMBDPO Photolysis. Photolysis of (2,4,6-trimethylbenzoyl)diphenylphosphine oxide (TMBDPO), which has also been studied, will be discussed in detail in another publication. Briefly, during the TMBDPO photolysis, the radical $(Ph)_2(O)P^\bullet$ is formed, which has a large HFI constant $a[^{31}P] \approx 36.5$ mT and negligible hyperfine coupling constants (≤ 0.1 mT) for the protons on the phenyl groups.[20] The main difference in the reactions of photolysis of TMPDE and TMBDPO is the lifetime of the excited triplet molecule, which is much shorter for the latter;[21−23] therefore, the triplet mechanism can contribute to the observed spin polarization. Indeed, the CIDEP signal of the trimethylbenzoyl radical, which was not observed during TMPDE photolysis, has been detected during photolysis of TMBDPO. Analysis of the experimental spectra and kinetics of $(Ph)_2(O)P^\bullet$ radicals showed the same trends and features as were shown for $(MeO)_2(O)P^\bullet$. The presence of TM is therefore not critical to the existence of low-field electronic−nuclear spin polarization.
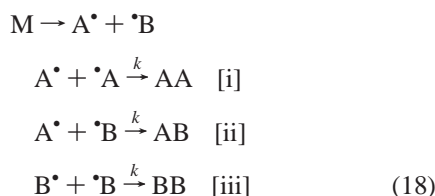
V. Conclusions

In conclusion, we would like to note that despite the fact that ENP has been detected for the specific case of radicals with large HFI constants the proposed polarization mechanisms should also work for radicals with HFI constant of 1.0−2.0 mT or for radicals with several HFI constants. For a radical with more than one nonzero HFI constant, the situation is more complicated, but zero-field ENP should still be observable.

The existence of strong spin polarization at low and zero magnetic fields, which can be detected using oscillating rf fields, is an important result. It will allow us to investigate mechanisms and kinetics of chemical reactions and molecular and spin dynamics of short-lived radical intermediates at low and zero magnetic fields. Particularly, studying low- and zero-field electronic−nuclear polarization using TREPR is a very good method for measuring low- and zero-field electronic−nuclear relaxation times, which is interesting information required for the analysis of much low-field magnetic resonance data.

Multiplet Electron−Nuclear Polarization

J. Phys. Chem. A, Vol. 106, No. 12, 2002 **2827**

Appendix

We begin by considering the photochemical reaction scheme below:

$$M \rightarrow A^{\bullet} + {}^{\bullet}B$$

$$A^{\bullet} + {}^{\bullet}A \xrightarrow{k} AA \quad [i]$$

$$A^{\bullet} + {}^{\bullet}B \xrightarrow{k} AB \quad [ii]$$

$$B^{\bullet} + {}^{\bullet}B \xrightarrow{k} BB \quad [iii] \qquad (18)$$

M is the precursor molecule, A and B are the radicals formed, and AA, AB, and BB are the recombination products of corresponding radicals. Let only the A radical contain a magnetic nucleus.

For the matrix of density $\hat{\rho}_A$ of radical A, the Liouville equation can be written in the following form:[24]

$$\frac{\partial \hat{\rho}_A}{\partial t} = (i\hat{\hat{L}}_A + \hat{\hat{R}}_A)\hat{\rho}_A(t) - [A]_0 \hat{\hat{K}}^A(t) \, \hat{\rho}_A(t) \times$$
$$\hat{\rho}_A(t) - [B]_0 \hat{\hat{K}}^B(t) \, \hat{\rho}_B(t) \times \hat{\rho}_A(t) \quad (19)$$

We rewrite the above equation in form more convenient for our calculations:

$$\frac{\partial \hat{\rho}_A}{\partial t} = (i\hat{\hat{L}}_A + \hat{\hat{R}}_A)\hat{\rho}_A - [A]_0 f_A(t) \, \hat{\hat{K}}^{AA} \, \hat{\rho}_A - [B]_0 f_B(t) \, \hat{\hat{K}}^{AB} \hat{\rho}_A$$
$$(20)$$

Here, the second and the third terms on the right side of equation describe the chemical decay of the radicals by second-order reactions, $[A]_0 = [B]_0 \equiv R_0$ are the initial concentrations of the radicals A and B, respectively, and $f_A(t)$ and $f_B(t)$ describe the time dependence of the concentrations of radicals A and B. $\hat{\hat{K}}^{AA}$ and $\hat{\hat{K}}^{BA}$ are

$$\hat{\hat{K}}^{AA} = \hat{\hat{K}}_r^{AA} + \hat{\hat{K}}_j^{AA}; \qquad \hat{\hat{K}}^{BA} = \hat{\hat{K}}_r^{BA} + \hat{\hat{K}}_j^{BA} \quad (21)$$

where matrixes $\hat{\hat{K}}_r^{AA}$ and $\hat{\hat{K}}_r^{BA}$ describe the chemical decay of the radicals in reactions [i] and [ii], respectively; matrixes $\hat{\hat{K}}_j^{AA}$ and $\hat{\hat{K}}_j^{BA}$ describe the formation of polarization in radical F pairs

The formal solution of eq 20 can be written as

$$\hat{\rho}_A(t) =$$
$$\exp(\int_0^t ((i\hat{\hat{L}}_A + \hat{\hat{R}}_A) - R_0 f_A(t')\hat{\hat{K}}^{AA} - R_0 f_B(t')\hat{\hat{K}}^{BA}) \, dt')\hat{\rho}_0$$
$$(22)$$

We designate $i\hat{\hat{L}}_A + \hat{\hat{R}}_A \equiv \hat{\hat{A}}$, and $R_0 f_A(t)\hat{\hat{K}}^{AA} + R_0 f_B(t)\hat{\hat{K}}^{BA} \equiv \hat{\hat{B}}$.

We now assume that the commutator $[\hat{\hat{A}}, \hat{\hat{B}}] \cong 0$. We will show below that matrix $\hat{\hat{B}}$ is taken close to the identity matrix; therefore, this approximation turns out to be valid, and eq 22 can be rewritten as

$$\hat{\rho}_A(t) =$$
$$\hat{\hat{T}}(t) \exp(-R_0\hat{\hat{K}}^{AA}\int_0^t f_A(t')dt' - R_0\hat{\hat{K}}^{BA}\int_0^t f_B(t')dt')\hat{\rho}_A(0) \quad (23)$$

where $\hat{\hat{T}}_A(t) = \exp((i\hat{\hat{L}}_A + \hat{\hat{R}}_A)t)$ is the operator of spin evolution.

Let $f_A(t) = f_B(t) = (1/(1 + 2kR_0t))$, which is obviously applicable for the reaction scheme used. Then, eq 23 is rewritten as

$$\hat{\rho}_A(t) = \hat{\hat{T}}(t)\left(\frac{1}{1 + 2kR_0t}\right)^{(\hat{\hat{K}}^{AA} + \hat{\hat{K}}^{BA}/2k)} \hat{\rho}_A(0) \quad (24)$$

Thus, the problem is reduced to the calculation of the spin-evolution operator $\hat{\hat{T}}(t)$ (i.e., to the solution of the following equation):

$$\frac{\partial \hat{\rho}_A}{\partial t} = (i\hat{\hat{L}}_A + \hat{\hat{R}}_A)\hat{\rho}_A \quad (25)$$

For the calculations of CIDEP kinetics in parallel rf field $B_1 \| B_0$, the energy absorbed at frequency ω can be calculated as

$$P(t) \propto B_1\omega \cdot Tr[\hat{S}_z \, \hat{\rho}(t)] \quad (26)$$

where $\hat{S}_z$ corresponds to a radical A.

For the calculations of CIDEP kinetics in transverse rf fields $B_1 \perp B_0$, eqs 19−25 have been rewritten for $(\hat{\rho}', \hat{\hat{L}}', \hat{\hat{R}}')$ in a rotating coordinate system. The energy absorbed at frequency ω, expressed through ρ', is

$$P(t) \propto B_1\omega \cdot Tr[\hat{S}_y \, \hat{\rho}'(t)] \quad (27)$$

where $\hat{S}_y$ corresponds to a radical A.

For both $B_1 \perp B_0$ and $B_1 \| B_0$, the Laplace transform has been used to solve eq 25 with the following numerical inverse Laplace transform. The matrix of HFI-induced relaxation has been taken from ref 17; $\hat{\hat{K}}' = (\hat{\hat{K}}^{AA} + \hat{\hat{K}}^{BA})/2k$ is an identity matrix, with the exceptions of $\langle 1|\hat{\hat{K}}'|1\rangle = \langle 2|\hat{\hat{K}}'|2\rangle = \langle 3|\hat{\hat{K}}'|3\rangle = 1 - \theta$ and $\langle 4|\hat{\hat{K}}'|4\rangle = 1 + \theta$ where θ is dimensionless phenomenological parameter characterizing CIDEP formation in diffusive RPs. In the case of $\theta \ll 1$, which corresponds to a small contribution to polarization formed in radical F pairs, the matrixes $\hat{\hat{K}}'$ and $\hat{\hat{B}}$ are very close to the identity matrixes, and the assumption made in eqs 22 and 23 that $[\hat{\hat{A}}, \hat{\hat{B}}] \cong 0$ is valid.

References and Notes

(1) Salikhov, K. M.; Molin, Yu. N.; Sagdeev, R. Z.; Buchachenko, A. L. *Spin Polarization and Magnetic Effects in Radical Reactions*; Molin, Yu. N., Ed.; Elsevier: Amsterdam, 1984.

(2) McLauchlan, K. A.; Yeung, M. T. *Specialist Periodical Report "Electron Spin Resonance"* **1994**, *14*, 32−62.

(3) Blattler, C.; Jent, F.; Paul, H. *Chem. Phys. Lett.* **1990**, *166*, 375.

(4) Bagryanskaya, E. G.; Ananchenko, G. S.; Nagashima, T.; Maeda, K.; Milikisyants, S.; Paul, H. *J. Phys. Chem. A* **1999**, *103*, 1127−11278.

(5) Ohara, K.; Terazima, M.; Hirota, N. *J. Phys. Chem. A* **1995**, *99*, 17814.

(6) Ohara, K.; Miura, Y.; Terazima, M.; Hirota, N. *J. Phys. Chem. A* **1996**, *101*, 605.

(7) Shushin, A. I. *Chem. Phys. Lett.* **1995**, *237*, 117.

(8) Till, U.; Timmel, C. R.; Hore, P. J. *Chem. Phys. Lett.* **1998**, *298*, 7−10. Timmel, C. R.; Till, U.; Brocklehurst, B.; McLauchlan, K. A.; Hore, P. J. *Mol. Phys.* **1998**, *95*, 71−77. Grissom, C. B. *Chem. Rev.* **1995**. *89*, 889. Canfield, J. M.; Belford, R. L.; Debrunner, P. G. *Mol. Phys.* **1996**, *89*, 889.

(9) Ananchenko, G. S.; Bagryanskaya, E. G.; Sagdeev, R. Z. *Chem. Phys. Lett.* **1998**, *282*, 450−455.

(10) Breit, G.; Rabi, I. I. *Phys. Rev.* **1931**, *38*, 2081.

(11) Alexandrov, I. V. *Zh. Eksp. Teor. Fiz.* **1971**, *60*, 1273. Adrian, F. J.; Monchik, L. *J. Chem. Phys*. **1979**, *71*, 2600. Adrian, F. J.; Monchik, L. *J. Chem. Phys*. **1980**, *72*, 5786.

(12) Doktorov, A. B.; Mikhailov, S. A.; Purtov, P. A. *Chem. Phys.* **1992**, *160*, 223−237.

(13) Purtov, P. A.; Doktorov, A. B. *Chem. Phys*. **1993**, *178*, 47−65.

(14) Purtov, P. A.; Doktorov, A. B.; Popov, A. V. *Chem Phys.* **1994**, *182*, 149.

(15) Griller, D.; Roberts, B. P.; Davies, A. G.; Ingold, K. U. *J. Am. Chem. Soc.* **1974**, *96*, 554−556.

(16) Koptyug, I. V.; Ghatlia, N. D.; Slugett, G. W.; Turro, N. J.; Ganapathy, S.; Bentrude, W. G. *J. Am. Chem. Soc*. **1995**, *117*, 9486−9491.

(17) Fedin, M. V.; Bagryanskaya, E. G.; Purtov, P. A. *Chem. Phys. Lett.* **2001**, *339*, 395−404.

(18) Burkey, T. J.; Lustzyk, J.; Ingold, K. U.; Wan, J. K. S.; Adrian, F. J. *J. Phys. Chem.* **1985**, *89*, 4286.

(19) Adrian, F. J.; Akiyama, K.; Ingold, K. U.; Wan, J. K. S. *Chem. Phys. Lett.* **1989**, *155*, 333.

(20) Landolt-Bornstein. New series, Group 2, Vol.11. Springer, Berlin. **1977**.

(21) Sumiyoshi, T.; Schnabel, W.; Henne, A.; Lechtken, P. *Polymer* **1985**, *26*, 141.

(22) Sumiyoshi, T.; Schnabel, W.; Henne, A. *J. Photochem.* **1985**, *30*, 63.

(23) Jockush, S.; Koptyug, I. V.; McGarry, P. F.; Sluggett, G. W.; Turro, N. J.; Watkins, D. M. *J. Am. Chem. Soc.* **1997**, *119*, 11495.

(24) Doktorov, A. B. *Physica* **1978**, *90A*, 109−136.